Journal of Fluids Engineering. Received March 23, 2023;
Accepted manuscript posted July 20, 2023. doi:10.1115/1.4062995

DROPLET FORMATION IN DYNAMIC STRATIFIED LIQUID-LIQUID SYSTEMS FOR SOLUTION-BASED DEPOSITION METHODS

Brett A. Prussack[1], Sean M. Foradori[2], Michael S. Arnold[3], Gregory F. Nellis[4], Arganthael Berson[5]

[1]Department of Mechanical Engineering, University of Wisconsin–Madison, 1513 University Ave, bprussack@wisc.edu

[2]Department of Materials Science and Engineering, University of Wisconsin–Madison, 1509 University Ave, foradori@wisc.edu

[3] Professor, Department of Materials Science and Engineering, University of Wisconsin–Madison, 1509 University Ave, michael.arnold@wisc.edu

[4] Professor, Department of Mechanical Engineering, University of Wisconsin–Madison, 1513 University Ave, gfnellis@engr.wisc.edu

[5] Lecturer and Scientist, Department of Mechanical Engineering, University of Wisconsin–Madison, 1513 University Ave, berson2@wisc.edu

ABSTRACT

The assembly of a 2D nematic liquid crystal at an interface between two liquids can be exploited to assemble densely packed and highly-aligned arrays of rod-like nanoparticles. This method is especially relevant to creating arrays of semiconducting carbon nanotubes (CNTs) for high-performance electronics. When a dense solvent containing CNTs flows over a less dense water subphase in a confined channel, the locally aligned arrays of nanoparticles align globally with the flow direction and can be transferred to the substrate. For large substrates and long channels, the dense solvent tends to slow and create a pool, which then drops through the interface and disturbs the delicate deposition process. Understanding this phenomenon is critical to improving and scaling up similar manufacturing processes. Here, data is collected, and an empirical model is developed to understand and predict the pooling behavior of a suspended fluid flowing over a less dense subphase. The model is demonstrated with two different solvents and proves to be accurate within +/- 15%. With a better understanding of the physics governing the system, the model is then used to suggest methods for minimizing pooling behavior.

Keywords: Experimental techniques, duct, channel, and pipe flows, films, free surface flows, free shear layers, suspensions, fluid instability, stability, and transition.

NOMENCLATURE

Bo	bond number
D_h	hydraulic diameter
g	gravitational acceleration
h	film thickness
H_f	head loss
L	front distance
L_c	capillary length
P	pooling parameter
Q	flow rate
v	velocity
w	channel gap width
x_{fd}	hydrodynamic fully developed length
θ	static contact angle
μ	dynamic viscosity
ρ	density
σ	surface tension

Subscripts

X_1	property at position 1
X_2	property at position 2
X_{cb}	chlorobenzene
X_{cf}	chloroform
X_{crit}	critical height
X_{sf}	supported fluid
$X_{w,air}$	property at water-air interface
$X_{w,cf}$	property at water-chloroform interface

Journal of Fluids Engineering. Received March 23, 2023;
Accepted manuscript posted July 20, 2023. doi:10.1115/1.4062995

1 INTRODUCTION

1.1 Background and Motivation

Carbon nanotube (CNTs) field effect transistors (CNFETs) have the potential to improve the performance and efficiency of semiconducting electronic devices. Logic devices constructed from highly aligned and densely packed arrays of CNTs will outperform similar Silicon based devices by 5 to 20 times in charge transport, efficiency and switching speed. [1-4]. The excellent properties of CNFETs can only be realized with densely packed, highly regular aligned arrays of nanotube films that are deposited on a substrate upon which FETs can be constructed. Several solution-based approaches have successfully created these nanotube arrays, including shear alignment [5], evaporative self-assembly [6], directed evaporation [7,8], DNA directed assembly [9], dimension-limited self-alignment [10], as well as the Langmuir Blodgett and Schaffer methods [6,11]. While all these methods show promise, significant advances in processing methods and technology are necessary to manufacture the high-quality arrays of CNTs demanded by CNFETs.

One particularly promising method of aligning CNTs and other rod-like nanoparticles utilizes the formation of a 2D nematic liquid crystal at a liquid-liquid interface [12]. Nanoparticles such as CNTs are dispersed in an organic solvent which is deposited on a water subphase. Self-assembly of a 2D nematic liquid crystal occurs at the liquid-liquid interface, where individual CNTs (approximately 1 nm in diameter and 0.7 μm in length) collect to form organized, locally aligned groups. The self-assembly that occurs at this interface results in densely packed, locally aligned arrays of CNTs.

Tangential Flow Interfacial Self-Assembly (TaFISA) is one novel method that utilizes liquid crystal formation at a liquid-liquid interface; this technique is the focus of this paper [13]. A simplified schematic of TaFISA is shown in Figure 1. The process utilizes a thin (3 mm) channel created between two parallel substrates that are partially submerged in a water reservoir and open on both ends. The fluid level between the plates forms a raised meniscus which is higher than the bulk water level. This is due to capillary rise between parallel plates, which explains that the cohesive forces between the liquid and the barrier acts to lift the liquid mass until the gravitational force is balanced.

A needle inserted into the channel delivers a solvent with dispersed carbon nanotubes (referred to as CNT ink) that flows on top of the raised water surface. As the CNT ink is injected, surface tension interactions between the water and the ink leads to the formation of a 2D nematic liquid crystal at the solvent-water interface. Nanotubes migrate from the bulk solvent (shown in red in Figure 1) to the water-solvent interface. This liquid crystal confines the nanotubes into densely packed, locally aligned arrays. With the addition of flow through the channel, viscous shear at the channel walls acts to align the CNT groups with the flow direction, creating a globally aligned nanotube film at the interface. As the substrates are lifted from the reservoir, the film is deposited onto the substrate at the ink/water interface [13].

Journal of Fluids Engineering. Received March 23, 2023;
Accepted manuscript posted July 20, 2023. doi:10.1115/1.4062995
Copyright (c) 2023 by ASME

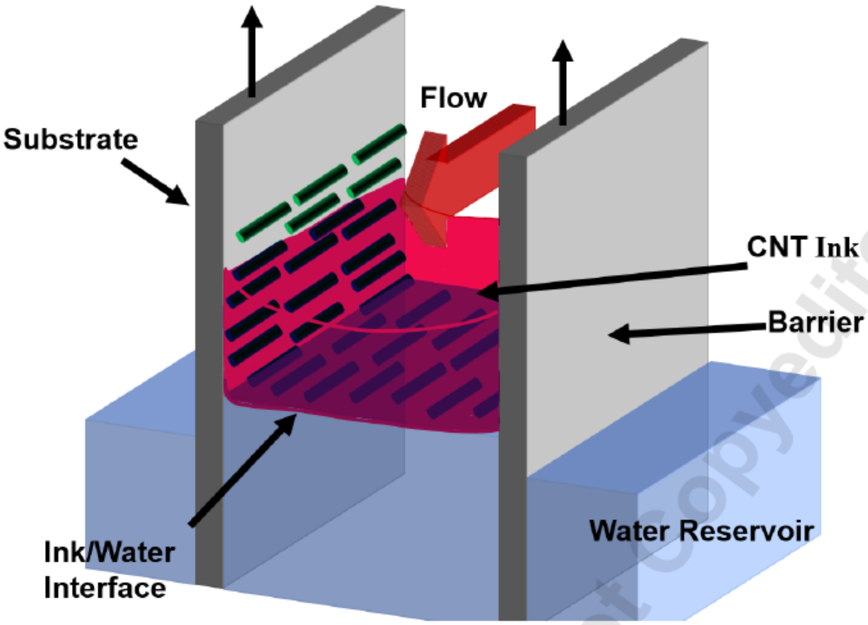

Fig. 1: Schematic showing interfacial assembly in TaFISA

TaFISA has demonstrated partial monolayer coverage with linear packing densities of 100 mm^{-1} measured perpendicular to the CNT's axis, and global alignment within ±6° over roughly 60% of a wafer [13]. Along the CNT axis, the CNTs arrange themselves nearly end to end, leaving negligible space between them. Full wafer coverage is a major benefit in device production, as it allows the entire surface of the substrate to be used to manufacture electronic devices. TaFISA has been conducted successfully on wafers from 2x2 cm^2 up to 6x10 cm^2, suggesting that the process is scalable. TaFISA relies on principles used in Langmuir-Blodgett and Schaefer methods [11] in combination with flow, but allows for much faster processing. The parameters and relationships that affect the deposition quality such as packing density and alignment are explored in detail by Jinkins [13] but are not a focus of this paper.

While methods like TaFISA show great potential, there are challenges that require attention before the process can be scaled and adopted by industry. Thus far, chloroform has been shown to be a good organic solvent for TaFISA; however, chloroform is denser than the sub-phase (water) that it rests on. Consequently, one of the major hurdles in TaFISA is suspending a denser solvent above a less dense sub-phase over long channel lengths while avoiding "pooling" phenomenon. Pooling is defined as an accumulation of solvent at a single location along the channel, so that the flow fails to reach the end of the channel. Once a pool begins to form, it creates a small depression which grows until it falls through the interface and sinks. Any amount of pooling in the suspended flow results in a failed deposition. Understanding, describing, and controlling the delicate suspension of a dense organic solvent on top of a water sub-phase is the focus of this paper.

Journal of Fluids Engineering. Received March 23, 2023;
Accepted manuscript posted July 20, 2023. doi:10.1115/1.4062995

1.2 Experimental Apparatus

The experimental apparatus used in this paper to study the TaFISA process is shown in Figures 2 and 3. The apparatus utilizes two aluminum frames which hold removable glass barriers that act as the channel. The transparent glass plates allow the behavior of the liquids in the channel to be observed during the deposition process. Parameters such as needle insertion height, ink film thickness, and water level variations and vibrations can be observed and measured. The aluminum frame is connected to a linear stage that lifts the fixture from the water trough at a controlled rate. The angle of the plates relative to the water surface is another process parameter that affects the deposition quality but not the flow stability in the channel. Note Figures 2 and 3 show the plates oriented 45° to the water surface, however here all data is collected in the vertical configuration, as shown in fig. 1. The process is also sensitive to the water level height in the channel. Therefore, as the plates are lifted from the trough a water leveling device is used to maintain a constant water level in the trough.

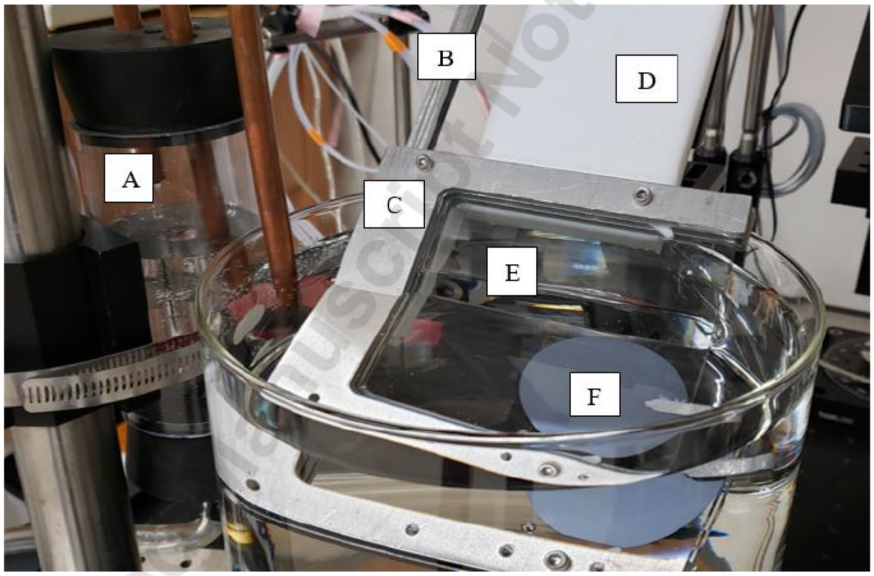

Fig. 2: Experimental apparatus. From left to right: (a) the water leveling device, (b) floating stationary post, (c) aluminum plates, (d) linear stage, (e) glass barriers, (f) sacrificial target substrate

The substrate, a P-type SiO_2 wafer with 90 nm thermal oxide, is held in place against the glass barrier using a small clamp positioned between the plates. This clamp covers a small (< 1 cm^2) portion of the substrate, which is the only area that cannot be coated with a nanotube film. The needle that delivers the ink is held in place using an aluminum post fixed relative to the plate motion; a series of holes in the post can be used to position the needle at various angles relative to the water level. The post fits within a small recess between the aluminum plates with the needle positioned between the glass barriers; as shown in Figure 3. The post acts as a barrier to

Journal of Fluids Engineering. Received March 23, 2023;
Accepted manuscript posted July 20, 2023. doi:10.1115/1.4062995
Copyright (c) 2023 by ASME

prevent backflow of the CNT ink out of the channel, directing all of the ink flow through the channel. The post is mounted to an independent and manually controlled linear stage that allows for accurate control of the needle height position relative to the water level and ensures that the needle remains stationary as the plate is lifted from the water.

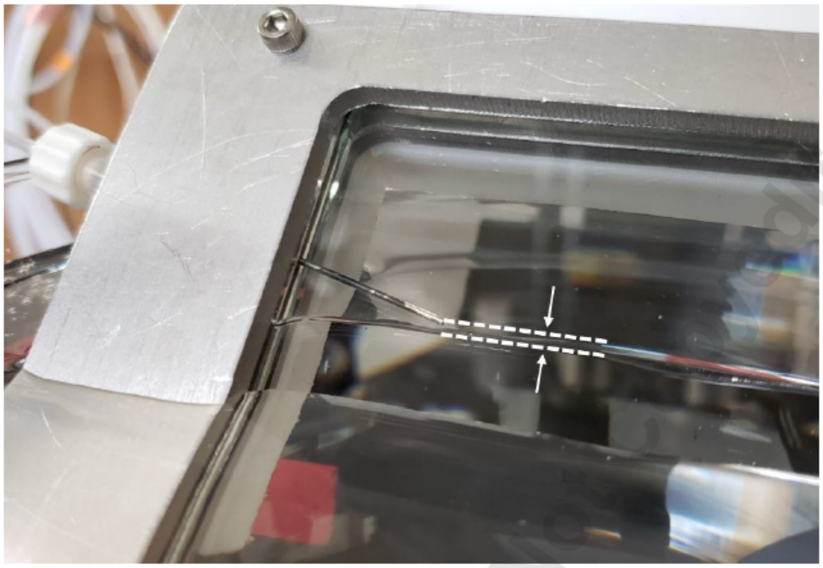

Fig. 3: Experimental apparatus showing the needle inserted into the channel. The needle insertion height is measured relative to the water interface. Shown here is a “negative” insertion height (i.e., the needle is above the water); an insertion height of “zero” corresponds to the center of the needle coinciding with the water interface.

1.3 Challenges Facing TaFISA

For TaFISA to be adopted on a large scale, the deposition process needs to be repeatable on the standard wafer sizes currently used in industry. These standard sizes range from diameters of 1 inch (25 mm) to 18 inch (45 cm) and therefore TaFISA will require channel lengths that are equal to or slightly larger than these desired wafer sizes. This paper focuses on scaling the channel length to accommodate a 4 in (10 cm) circular substrate, an important incremental increase from traditional TaFISA [13]. As the ink flows, friction with the channel walls and the water subphase acts to slow the moving ink layer which makes it difficult for the ink to reach the exit. This is particularly true at large channel lengths and low flow rates. Experiments with longer channel lengths show that the ink may collect in the channel at some intermediate position and form droplets (or pools). Eventually the pool becomes large enough that it sinks and falls below the water surface, causing large disturbances of the water surface within the channel and ruining the deposition process. Once an ink pool is established, the flow across the channel is disrupted and the ink will consistently sink at that location; this is shown by the sequence of images in Figure 4.

Journal of Fluids Engineering. Received March 23, 2023;
Accepted manuscript posted July 20, 2023. doi:10.1115/1.4062995

Fig. 4: Evolution of droplet formation in the TaFISA channel. The scalebar shown is 1 cm

The issue of pooling and sinking ink must be addressed in order to allow an ink flow to be established through the entire length of a long channel in a consistent and controllable manner. To scale TaFISA and other solution-based processing methods to larger wafers, it is important to develop a general understanding of the behavior of the fluids involved (CNT ink and water) within the channel and the impact of various operating parameters on the achievable front distance (i.e., the distance that the CNT ink travels before pooling).

The flow within the channel in TaFISA can be classified as a stratified flow of immiscible liquids between parallel plates. In this case, the lower fluid phase is a deep reservoir of stationary water. The upper fluid is a higher density layer of liquid flowing through the channel; this flow is bounded by the 2 glass plates but remains open to the atmosphere above and at the exit. Research on similar stratified gas-liquid and liquid-liquid flow has focused on internal pipe flow, primarily with the less dense fluid on top [14]. The primary focus of these prior studies is the characterization of the interface that separates the two fluids and the prediction of pressure drop and liquid hold-up. Few studies have been done on stratified liquid-liquid flow between parallel plates and those that do exist focus on situations in which the less dense liquid is supported on a higher density subphase. For example, the work by Keulegan [15] focuses on the interface behavior in this situation, specifically the formation of waves and the resulting mixing that occurs as a function of the flow rate. This study shows that the flow velocity, fluid density, and viscosity all play a substantial role in the interface behavior. For all the conditions that were tested here in the TaFISA channel, no waves or other interfacial instabilities are observed.

Another area of research that is relevant to the pooling and sinking behavior observed during TaFISA is the gravitational stability of liquid lenses that are supported on a liquid subphase. Research in this field primarily focuses on the wetting/spreading behavior of lower density liquid lenses on a higher density subphase, with few studies discussing the opposite case [16,17]. Other studies investigate the stability of water droplets and solid cylinders suspended on a liquid subphase [18,19]. Results from these studies show that interfacial surface tension forces and contact angles play a significant role in the stability of the suspended liquid; however, none of these works address the details of pooling and sinking of the upper fluid. Additionally, this prior work has been carried out on static systems and does not consider the dynamic forces that arise in a flowing situation. To the authors' knowledge, the stability of a dense liquid film flowing over a less dense liquid subphase between parallel plates has not been previously investigated.

Journal of Fluids Engineering. Received March 23, 2023;
Accepted manuscript posted July 20, 2023. doi:10.1115/1.4062995

This paper is divided into an experimental section in which the experimental procedure and data collection process are described. The data are then presented, and some observations are identified in order to motivate the subsequent analysis. The results and discussion section investigates the dominant forces associated with the stratified flow that exists within the channel and identifies relevant dimensionless numbers that are used to define a critical condition where pooling behavior is likely to occur. This critical condition is used in the context of a simple model to develop a correlation for front distance. Finally, the results from the correlation are used to suggest methods for increasing front distances for longer channel widths.

2 MATERIALS AND METHODS

2.1 Data Collection

The pooling and sinking behavior of a suspended, high-density liquid supported on a lower-density liquid and flowing in a thin channel is studied using the experimental apparatus developed for TaFISA that is described in Section 1.2 and shown schematically in Figure 5.

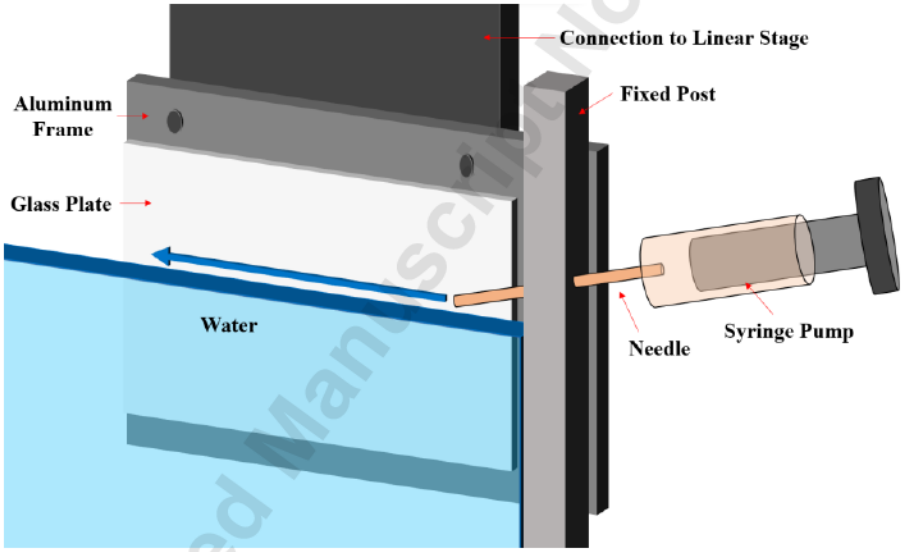

Fig. 5: Schematic of experimental apparatus with the near plate and barrier omitted

The channel is created between two 10 cm square glass plates that are separated by spacers that control the channel gap. The glass plates are held in an aluminum frame which is attached to a motorized linear stage. The plates are partially submerged vertically in a trough filled with clean, 1 MΩ water. The water contact line is visible through the transparent glass plates. The ink (chloroform) is introduced into the channel through a 1 mm inner diameter needle that is held in a post at the entrance of the channel. The needle is held at a 5° angle from the horizontal and centered in the channel. The chloroform flow rate is controlled using a NEXUS 3700 syringe pump. The data collection process starts by partially submerging the plates in water, after which the needle height is set using a linear stage to

Journal of Fluids Engineering. Received March 23, 2023;
Accepted manuscript posted July 20, 2023. doi:10.1115/1.4062995

move the post vertically. A flow rate is selected, the syringe pump is activated, and ink flow is initiated. The behavior of the interface is recorded using a Dino-Lite Basic AM2111 camera. During each test, either the ink front reaches the end of the channel and exits successfully, or the front slows and pools before the exit. In the latter case the front distance (i.e., the distance between the point the ink exits the needle and the point that it pools) is recorded. After each run, the plates are fully removed from the trough with the linear stage and the ink is allowed to evaporate from the plates and the water surface. The plates are then re-inserted, and the process is repeated for the next test.

A scale is attached to the plate to allow the front distance to be measured accurately based on video recorded during the process. The pool typically has a width of roughly 1 cm, and the pooling location is taken to be the center of the pool. Measurements are only recorded for tests during which pooling and sinking occur. For tests where the ink successfully reaches the far end of the channel, a front distance cannot be measured and therefore these trials were not considered in the data collection. Under some conditions, pooling initially occurs a short distance from the needle and the location of pooling subsequently slowly moves towards a maximum value. Under these conditions, the front distance was recorded after the pooling and sinking location has stopped moving.

The front distance as a function of needle height was initially studied to determine how sensitive the process is to this parameter. A needle height of zero corresponds to the bottom edge of the needle just contacting the water surface. Any further movement into the water is taken to be an increase in needle height. Figure 6 shows the front distance as a function of needle height measured at flow rates of 4 mL/min and 6 mL/min for a 1.5 mm plate separation. For a given flow rate, fig. 6 shows that the front distance remains constant to within about 0.5 cm regardless of needle height, indicating that the effect of this parameter is relatively insignificant. For the remainder of the data collected, a needle height of 0.75 mm is used. This leaves the needle partially submerged in water. Above 1.5 mm, the needle is fully submerged which causes the chloroform to sink immediately after exiting the needle.

Journal of Fluids Engineering. Received March 23, 2023;
Accepted manuscript posted July 20, 2023. doi:10.1115/1.4062995

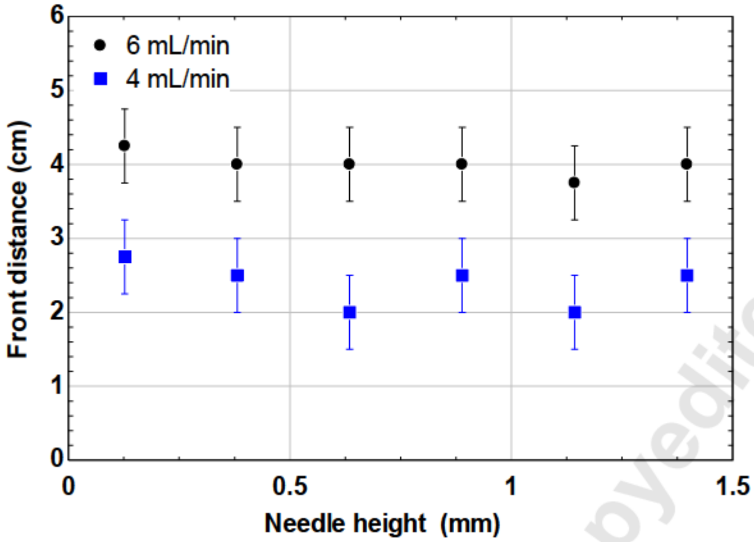

Fig. 6: Front distance as a function of needle height for two different flow rates

Flow rates ranging from 2 mL/min to 8 mL/min were used in 1 mL/min increments. Above 8 mL/min, the flow consistently reaches the end of the channel. Channel gaps between 1.5 mm and 3 mm were tested in 0.5 mm increments. Figure 7 depicts the plates and post from above. Above a channel gap of 3 mm the post holding the needle no longer occupies the entire channel gap and a significant backflow of ink out of the channel is observed due to the gap between the post and plates; as a result, it is not possible to accurately measure the flow rate that passes through the channel. Below a channel gap of 1.5 mm, there is interference between the needle and the channel. Each combination of channel gap and flow rate was tested three times and the results of these three tests are averaged.

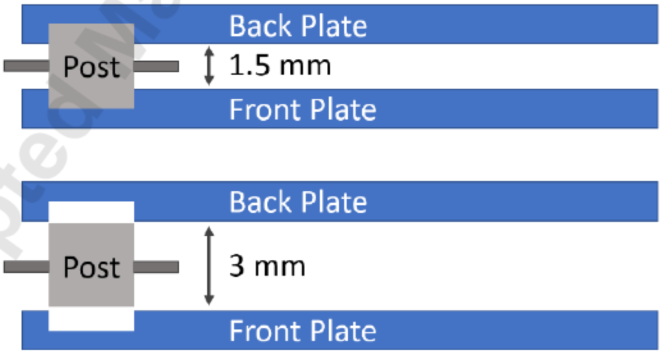

Fig. 7: Schematic of experimental setup demonstrating the lower and upper limits of channel widths

The parameters that are held constant in this experiment include the static contact angle of the plates with respect to water, needle insertion height, needle diameter and needle angle; the values of these parameters are summarized in Table 1. The static contact

Journal of Fluids Engineering. Received March 23, 2023;
Accepted manuscript posted July 20, 2023. doi:10.1115/1.4062995

angle is measured by placing a small drop of de-ionized water on a horizontal plate surface. The resulting contact angle is measured at five locations on the plate surface and these values are averaged. Images are taken and measurements of the contact angle are carried out using MATLAB. Prior to testing, the glass plates are rinsed with isopropyl alcohol to remove any large contaminants, then UV Ozone treated to remove any organic contaminants and to make the surface hydrophilic. This treatment yields a consistent static contact angle for water that is near 10°. Measurements of the contact angle before and after the trials show that the contact angle is unaffected by repeated trials with ink and clean water.

2.2 Data Analysis

All data were collected in a single session according to the data collection procedure described in the previous section. Three data points for each channel width and flow rate combination were recorded and averaged. The raw data are presented in Table 2 and the averaged values are presented in Table 3. Datapoints labeled “n/a” represent conditions where the flow reaches the end of the channel, and no pooling occurs. It is apparent that there is some variation in the front distance measured for a given set of conditions. One possible explanation is inherent inconsistencies in the contact angle (±3°) that are observed in solid-liquid systems [20]. The uncertainty associated with the measured data is estimated as twice the standard deviation (s) of the trials, which is calculated by taking the square root of the variance of each group of three data points. The average standard deviation for all datapoints is found to be 0.26 cm so the uncertainty is taken to be 0.52 cm.

Figure 8 shows the measured front distance as a function of flow rate for several channel widths. The relationship between front distance and flow rate appears to be approximately linear for a given channel width. Intuitively, increasing flow rate should lead to a larger front distance as more momentum is associated with the liquid leaving the needle which allows it to resist slowing down and eventually pooling.

Journal of Fluids Engineering. Received March 23, 2023;
Accepted manuscript posted July 20, 2023. doi:10.1115/1.4062995

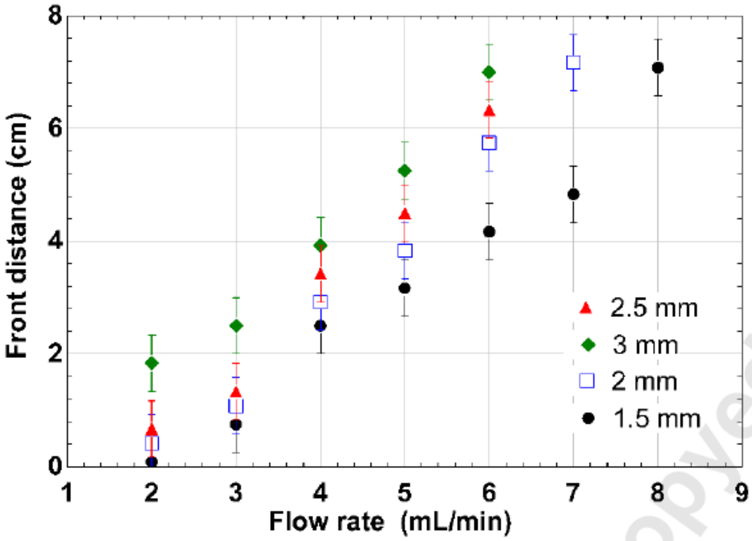

Fig. 8: Front distance as a function of flow rate for various values of the channel width

Figure 9 shows the front distance as a function of channel width for various flow rates. Flow rates of 7 and 8 mL/min were excluded, as there were fewer data points for these high flow rates since the flow successfully reached the end of the channel in many of these trials. The effect of channel width is less dramatic than flow rate, but in general a larger channel corresponds to a longer front distance.

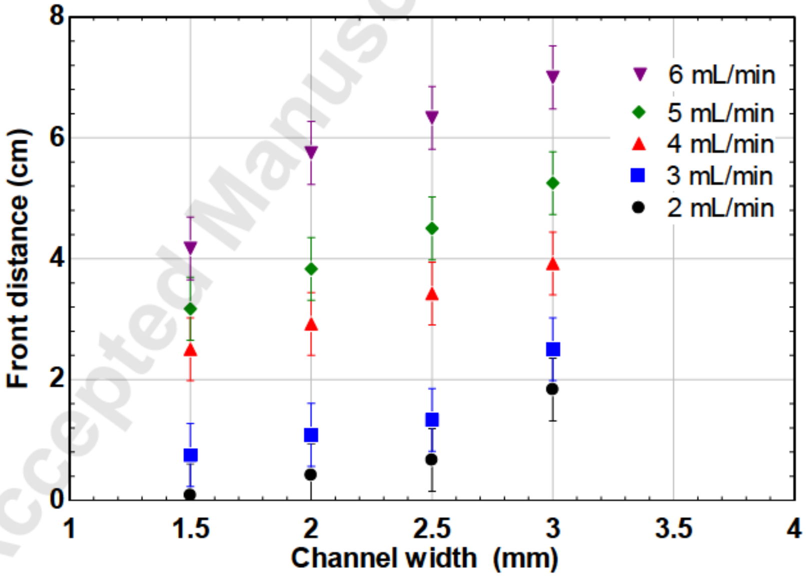

Fig. 9: Front distance as a function of channel width for chloroform

Evidently, increasing either flow rate or channel width has a positive effect on front distance. To understand this relationship, the forces that govern the flow in the channel are identified and used to create a simple scaling model describing the achievable front

Journal of Fluids Engineering. Received March 23, 2023;
Accepted manuscript posted July 20, 2023. doi:10.1115/1.4062995

distance in the subsequent section. This model is used together with the data to develop a semi-empirical relationship for the front distance.

3 RESULTS AND DISCUSSION

3.1 Model Derivation

A working model of suspended fluid flow in a thin channel can be used to understand and optimize the TaFISA process as well as other, similar solution-based materials processing methods. Such a physics-based model will help to design and scale the process without expensive trial and error. The dominant force acting to support the suspended fluid layer is the surface tension force at the ink-glass interface. The force acting to induce pooling is gravity. The dimensionless number that compares the ratio of the gravity to the surface tension forces is the Bond number, which is generally defined according to:

$$Bo = \frac{\rho\, g\, L^2}{\sigma} \tag{1}$$

The Bond number is often used to understand the behavior of a droplet or a bubble. However, the Bond number is also relevant for liquid-liquid systems or for systems considering only a single fluid [21]. In models of dispersed multiphase fluid flows, the length scale is often taken to be the dimension of the bubbles, droplets, or particles that are suspended in the flow [22]. However, the situation studied here contains none of these discrete elements and instead the square of the length scale is replaced by the product of the radius of curvature of the meniscus at the wall, approximated as the channel width divided by the cosine of the solvent-barrier contact angle, and the ink layer height, which is proportional to the volume of the liquid that is being supported. The density is replaced by the density difference between the dense ink and less dense water, $\Delta\rho$, which is the parameter that gives rise to the gravitational force. A modified Bond number is defined for this case according to:

$$Bo = \frac{\Delta\rho\, g\, w\, h}{2\, \sigma \cos(\theta)} \tag{2}$$

where σ and θ are the surface tension and contact angle, respectively, of the supported fluid with the barrier. The surface tension term is multiplied by 2 because the force is exerted on either side of the meniscus by both plates.

The modified Bond number provides a criterion for pooling; a critical Bond number of unity is assumed because in this condition the competing forces are closely balanced [21]. Situations dominated by surface tension have $Bo < 1$ while those dominated by gravity have $Bo > 1$. Equation (3) can be rearranged and simplified to solve for the maximum film thickness that a given interface can support, or the critical thickness where the fluid layer becomes unstable:

$$h_{crit} = \frac{2\, \sigma \cos(\theta)}{\Delta\rho\, w\, g} \tag{3}$$

Journal of Fluids Engineering. Received March 23, 2023;
Accepted manuscript posted July 20, 2023. doi:10.1115/1.4062995

This definition is only physically meaningful for immiscible or insoluble fluids that avoid mixing, such as the strong solvents and water used here. It should also be noted that this definition is physically meaningful for channel geometries and films that result in a continuously curved meniscus (i.e., one in which the radius of curvature is directly related to the gap width). The capillary length is a fluid property that predicts the behavior of menisci by relating gravity and surface tension forces [23, 24]. The assumption that the meniscus is curved is reasonable at small channel widths, where the radius of the resulting meniscus (*w*/2) is smaller than the capillary length, given by:

$$L_c = \sqrt{\frac{\sigma}{\Delta\rho\, g}} \tag{4}$$

where $\Delta\rho$ is the difference in density between the fluids of interest, in this case the solvent and water. The capillary length for chloroform is 1.35 mm, indicating the model becomes less valid at channel widths greater than 2.7 mm. At larger channel width, the solvent tends to spread to form a flat layer that behaves differently from a continuously curved meniscus. To account for this change in interface shape that occurs for large widths, the parameter w in Eq. (3) is replaced with the minimum of twice the capillary length and the channel width. Thus, at large channel widths, where the interface shape no longer changes drastically with gap width, the radius of curvature is determined by twice the capillary length divided by the cosine of the contact angle. Eq. (3) is modified accordingly:

$$h_{crit} = \frac{2\,\sigma\,\cos(\theta)}{\Delta\rho\, g\,[min\,(w, 2L_c)]} \tag{5}$$

The supported ink layer is flowing on top of a water sub-phase (in the direction that is into the page in Figure 9). The actual film thickness is governed by the flow rate of the injected fluid and its velocity according to continuity. The fluids that are used as the solvents are incompressible and therefore continuity dictates that the volumetric flow rate at any point in the channel is constant. Thus, the supported fluid layer thickness h_{film} is given by:

$$h_{film} = \frac{Q}{w\,v} \tag{6}$$

where w is the gap width and v is the average (or bulk) local velocity. Figure 10 shows an exaggerated image that will result from the slowing liquid front (due to friction) causing a growing ink layer in the channel; eventually, the critical film height is reached, and the supported fluid begins to pool. The distance between this pooling location and the injection point is referred to as the front distance, *L*, and should be maximized to allow larger deposition areas.

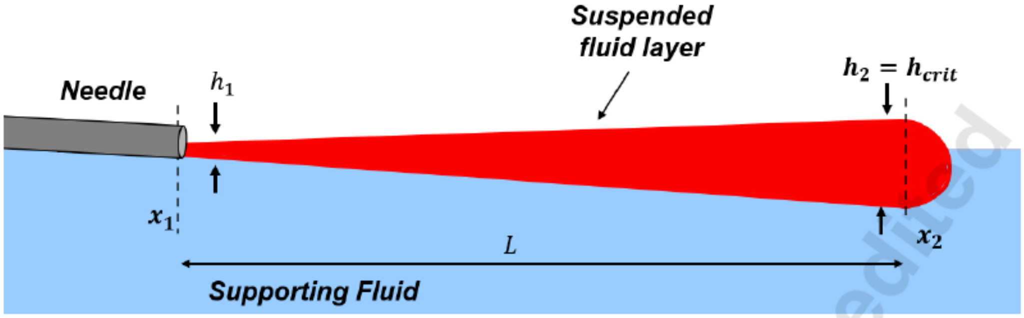

Fig. 10: The supported fluid layer slows as friction acts to decelerate the front which causes its height to grow; eventually the critical height is reached which causes pooling to occur

It is worth noting that the ink trajectory shown in fig. 10 changes direction to follow the water surface after exiting the needle. This is a reasonable approximation because the angle of the needle is small, only 5°, so that the vertical component of the ink velocity is negligible, and it changes direction to follow the water surface immediately upon exiting the needle. The location where the ink is injected is x_1 and the film thickness at this location (h_1) is equal to the diameter of the needle at the start of the channel. The location downstream where the ink will pool is x_2 and the film thickness at this location is the critical film thickness. The front distance, *L*, is the difference between these locations:

$$L = x_2 - x_1 \tag{7}$$

The conservation of energy equation is applied between points x_1 and x_2 along a streamline in the channel separated by distance *L,* assuming that the flow is steady, and the fluid is incompressible.

$$\frac{P_1}{\rho\, g} + \frac{v_1^2}{2g} + z_1 = \frac{P_2}{\rho\, g} + \frac{v_2^2}{2g} + z_2 + H_f \tag{8}$$

As the fluid flows, viscous friction forces with the walls of the channel and the liquid-liquid interface act to decelerate the fluid. These losses are captured by the parameter H_f, the head loss due to friction. The channel is open to the atmosphere, so P_1 and P_2 can be assumed to be equal. The vertical height change is assumed to be small so the elevations z_1 and z_2 are also assumed to be equal. Therefore, the energy balance can be simplified to:

$$\frac{v_1^2}{2g} = \frac{v_2^2}{2g} + H_f \tag{9}$$

The head loss due to friction is approximated using the Darcy-Weisbach equation for pressure head loss in a pipe [25], where f_d is the Darcy-Weisbach friction factor.

Journal of Fluids Engineering. Received March 23, 2023;
Accepted manuscript posted July 20, 2023. doi:10.1115/1.4062995

$$H_f = f_d \frac{L}{w} \frac{v_{avg}^2}{2g} \tag{10}$$

The velocity used in Eq. (10) is the average bulk velocity in the channel (the average of the velocities at locations 1 and 2):

$$v_{avg} = \frac{v_1+v_2}{2} \tag{11}$$

Equations (6) through (11) can be simplified and rearranged to solve for the front distance normalized by the channel width:

$$\frac{L}{w} \approx \frac{4}{f_d}\left[\frac{1}{h_1^2} - \frac{1}{h_{crit}^2}\right]\left[\frac{1}{h_1} + \frac{1}{h_{crit}}\right]^{-1} \tag{12}$$

For laminar fully developed flow, the friction factor will be inversely proportional to the Reynolds number:

$$f_d = \frac{k}{Re} \tag{13}$$

where *k* is a constant that depends on the channel geometry. For example, for fully developed flow between parallel plates *k* = 96 when the Reynolds number is defined based on the hydraulic diameter [25]. The Reynolds number used here is defined using the channel width, *w*, as the characteristic length:

$$Re = \frac{Q\,\rho}{\mu\,h} = \frac{\rho\, v_{avg}\, w}{\mu} \tag{14}$$

where μ is the dynamic viscosity of the supported fluid and v_{avg} is the average velocity given by Eq. (11). Substituting equations (13) and (14) into Eq. (12) and simplifying yields an approximate relationship for the dimensionless front distance:

$$\frac{L}{w} \approx \frac{2\,Q\,\rho_{sf}}{k\,\mu_{sf}}\left[\frac{1}{h_1^2} - \frac{1}{h_{crit}^2}\right]\left[\frac{1}{h_1} + \frac{1}{h_{crit}}\right]^{-1} \tag{15}$$

For simplicity, the right side of Equation (15), less the constant *k*, is called the pooling parameter, *P*

$$P \approx \frac{2\,Q\,\rho_{sf}}{\mu_{sf}}\left[\frac{1}{h_1^2} - \frac{1}{h_{crit}^2}\right]\left[\frac{1}{h_1} + \frac{1}{h_{crit}}\right]^{-1} \tag{16}$$

The approximate relationship for the dimensionless front distance is then:

$$\frac{L}{w} = \frac{P}{k} \tag{17}$$

In the following section, the relationship between dimensionless front distance and pooling parameter is examined using the experimental data and a correlation is developed for front distance.

3.2 Examination of Experimental Data using the Model

A variety of organic solvents can be used to disperse nanoparticles in solution to facilitate transfer of particles to a substrate. Therefore, front distance data were also collected for chlorobenzene using the same method described in Section 2.1 for the chloroform

Journal of Fluids Engineering. Received March 23, 2023;
Accepted manuscript posted July 20, 2023. doi:10.1115/1.4062995

testing. The same range of flow rates were tested with channel widths of 1.5 and 2 mm. The properties of chloroform and chlorobenzene are given in Table 4.

It is worth noting here that it is assumed that the properties of the bulk fluid are not significantly affected by the addition of nanoparticles, in this case single wall carbon nanotubes (SWCNTs). A typical concentration of SWCNTs for TaFISA is 100 µg/mL, which corresponds to a percentage by weight in chloroform of 6.7%. Literature suggests that surface tension of solutions containing multi-wall CNTs (MWCNTs) which are larger in diameter and length, only slightly affects the bulk fluid surface tension. In the case of [26], a 5 wt. % addition of MWCNTs corresponds to a 1% decrease in surface tension of the bulk ethylene glycol solution. Regarding other fluid properties such as dynamic viscosity, the addition of nanoparticles may have a significant effect. The work by Xiaoke demonstrates that with 5 wt. % addition of MWCNTs, the viscosity of the base fluid (water) increases by 22 times. This effect is likely sensitive to other factors such as the base fluid, the nanoparticle size, and the presence of a stabilizing agent to maintain individualization of the nanoparticles [27]. In the author's experience, experimentation with the addition of 100 µg/mL of SWCNTs has not demonstrated a significant deviation from the results shown here. It is likely that in other systems with different base fluids and nanoparticle types and concentrations, the nanoparticle concentration will have a significant effect on the fluid properties. The dimensionless front distance measured for both chloroform and chlorobenzene are plotted as a function of the pooling parameter, *P*, in Figure 11.

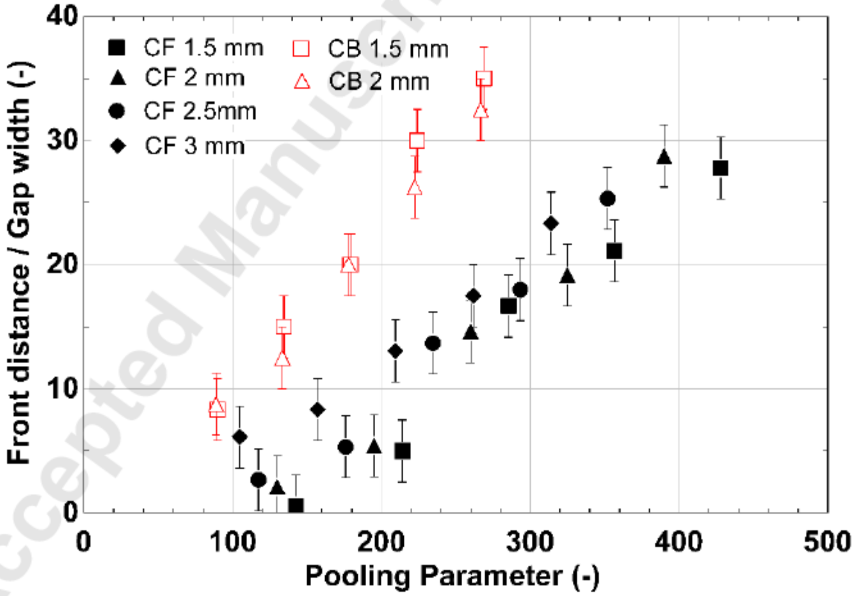

Fig. 11: Dimensionless front distance as a function of pooling parameter for chloroform (black) and chlorobenzene (red)

Journal of Fluids Engineering. Received March 23, 2023;
Accepted manuscript posted July 20, 2023. doi:10.1115/1.4062995

Notice that the data for each fluid collapse separately with an approximately linear relationship. Ideally, the data for both fluids should collapse to a single line since the model considers fluid properties. This suggests that the friction factor coefficient, *k*, may not be identical for both fluids. Therefore, it is worth evaluating the assumptions made about the friction factor *k* in Eq. (13) to confirm that they are appropriate. The use of a single *k* value assumes that the flow in each case is laminar and fully developed. Even for high flow rates, the Reynolds number for both fluids remains in the laminar regime. To evaluate the assumption that flow is fully developed, the hydrodynamic entry length for internal flow [28] is computed according to:

$$x_{fd} \approx 0.06\, Re\, D_h \tag{18}$$

where D_h is the hydraulic diameter.

By inspection of Eq. (18) and the fluid properties, chlorobenzene becomes fully developed more quickly than chloroform, by approximately a factor of two. Therefore, it is reasonable that the friction factor parameter *k* will be smaller for chlorobenzene than it is for chloroform, where the hydrodynamic entry length is a significant fraction of the channel length. The geometry associated with the flow in this experiment does not conform to a typical, confined internal flow and therefore it is not possible to precisely predict the *k* values based on literature. Here, the friction factor *k* absorbs the effects of unknown factors such as the impact developing length in this unique channel geometry.

Using the data in Figure 11, it is found that the most appropriate value of *k* for chlorobenzene is k_{cb} = 10 whereas the friction coefficient for chloroform is k_{cf} = 20. These values are chosen because they minimize the deviation of the data collected for each fluid. Note these differ by a factor of two; this difference may be related to the difference in fully developed length explained by Eq. (18), or because many of the assumptions made in developing the model introduce error, which is absorbed into *k* for each fluid. Using these parameters, the measured dimensionless front distance as a function of the ratio of the pooling parameter to the friction factor parameter *k*, Eq. (17), is shown in Figure 12. Also shown in Figure 12 is the best fit and ±15% deviation lines.

Journal of Fluids Engineering. Received March 23, 2023;
Accepted manuscript posted July 20, 2023. doi:10.1115/1.4062995

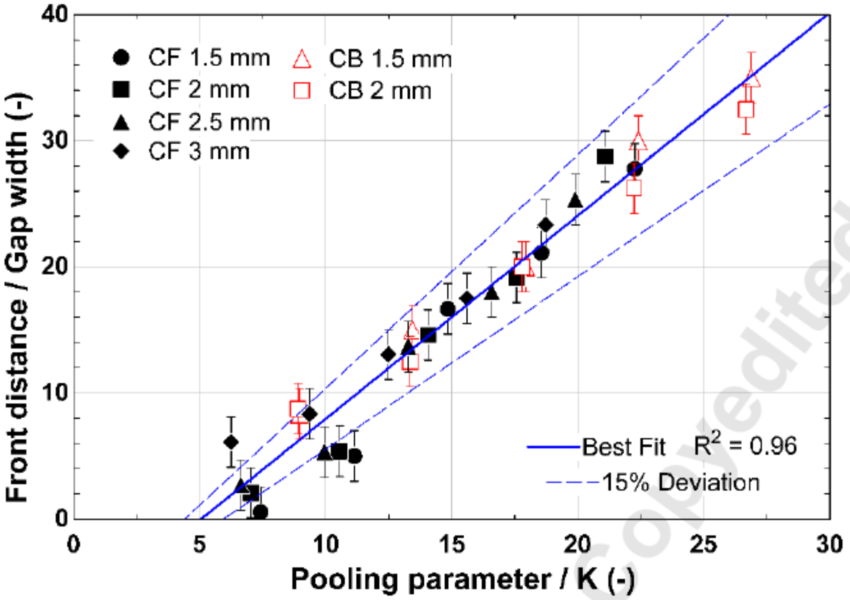

Fig. 12: Front distance normalized by gap width as a function of the pooling parameter for chloroform and chlorobenzene

Using these values of the friction coefficient, the data for both fluids collapse to a single line. Over 80% of the data fall within ±15% of the best fit line, suggesting a strong relationship between dimensionless front distance and the pooling parameter divided by the friction coefficient. It is worth noting that at low flow rates the effects of friction and surface tension are relatively high, and these are less controllable, leading to a lower degree of certainty, as seen in Figure 12. The best fit line yields a correlation for front distance as a function of gap width, pooling parameter, and the friction coefficient:

$$L = w\left[1.61\left(\frac{P}{k}\right) - 8.14\right] \tag{19}$$

$$P \approx \frac{2\,Q\,\rho_{sf}}{\mu_{sf}}\left[\frac{1}{h_1^2} - \frac{1}{h_{crit}^2}\right]\left[\frac{1}{h_1} + \frac{1}{h_{crit}}\right]^{-1} \tag{16}$$

$$k_{cb} = 10, k_{cf} = 20$$

A linear curve fit to the data yields the best fit line given in Eq. (19) and has a slope of 1.61 which deviates significantly from the predicted slope of one in the analytical solution given by Eq. (17). This most likely stems from the fact that the model only approximates the dominant forces governing the behavior in the channel, and many assumptions are made in order to simplify its derivation. There are several potential reasons as to why the slopes differ. The first is that the Darcy-Weisbach friction loss term in Eq. (10) assumes that the flow is fully developed and laminar. It can be assumed that the flow is laminar, however the developing length for chloroform and chlorobenzene at 6 mL/min and 3 mm width is 5 and 2.5 cm respectively, both of which are a significant portion of the channel and would likely cause behavior different from the ideal scenario described by Eq. (10). A second potential reason for the

Journal of Fluids Engineering. Received March 23, 2023;
Accepted manuscript posted July 20, 2023. doi:10.1115/1.4062995

deviation includes the use of an average velocity when calculating friction instead of integrating to solve for friction loss as a function of the velocity. A third potential deviation is because here friction is only considered between the solvent and the barriers, and not with the underlying water surface. Any or all three of these factors likely account for the deviation observed in the slope.

Equation (19) describes the relationship governing the front distance for a supported fluid layer flowing between parallel plates, and is dependent on the channel geometry w, a dimensionless pooling parameter P, and the friction coefficient parameter k, which equals 10 and 20 for chlorobenzene and chloroform respectively. Recall the pooling parameter, defined in Eq. (16) is a function of fluid properties, the initial fluid layer thickness, h_1 (or more simply the inlet diameter), and the critical fluid layer thickness, h_{crit} which is determined using the modified Bond number. The correlation simplifies the complex relationship between the buoyancy, surface tension, gravity, and friction forces as they affect the front of a flowing suspended fluid. It also helps to identify the impact of parameters such as channel width and flow rate on pooling behavior. Understanding these relationships is an important step in scaling solution-based materials processing methods that rely on liquid-liquid interfaces, such as TaFISA. The next section applies the correlation to make predictions about front distance and to suggest methods for avoiding pooling.

3.3 Methods to Improve Front Distance

The objective of the experimental and modeling work in this paper is to understand the behavior of a dynamic front confined in a thin channel and to identify methods that can be used to increase front distance. Figure 13 shows the front distance as a function of gap width for various values of flow rate predicted by the correlation given in Eq. (19), overlayed with experimental data.

Journal of Fluids Engineering. Received March 23, 2023;
Accepted manuscript posted July 20, 2023. doi:10.1115/1.4062995

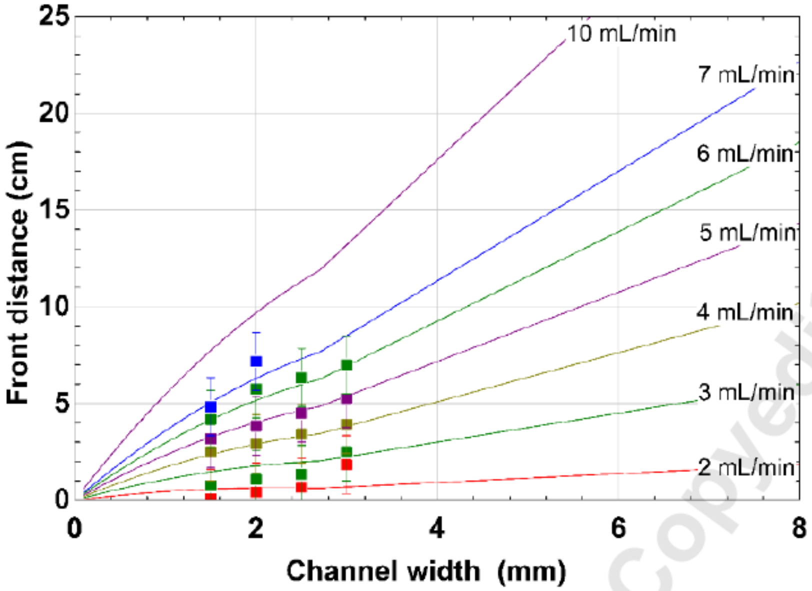

Fig. 13: Correlation results from Eq. (17) and data for chloroform front distance as a function of the channel width for various values of flow rate

The correlation predicts an inverse parabolic relationship between front distance and channel width until the channel width becomes larger than $2L_c$, at which point front distance begins increasing linearly. This relationship can be explained conceptually by the balance between friction and surface tension forces. Small channel widths lead to much higher losses due to friction that act to quickly decelerate the front and encourage a growing fluid layer. As channel width increases, losses due to friction are less significant and the front can move more easily through the channel. As channel width increases further, the surface tension forces remain relatively constant, and the fluid behaves as it would on a featureless water surface.

The practical application of the model lies in its ability to predict the general trends that are observed as flow rate, channel width, and fluid properties are varied. For example, if a given deposition method requires suspended flow across a 10 cm substrate, Figure 13 can be used to select a flow rate and channel width combination favorable to the deposition parameters. This example case would suggest a flow rate near 7 mL/min and a channel width near 4 mm.

Solution based deposition methods like TaFISA often depend heavily on the fluid conditions during the deposition process. This usually means operating within the laminar flow regime in order to avoid turbulent eddies near the interface, which can lead to poor deposition quality [13]. It follows that in many cases higher flow rates are undesirable, despite being one of the simplest methods to increase front distance. For example, an 18 cm substrate might suggest flow at 10 mL/min in a 5 mm channel width to reach the

Journal of Fluids Engineering. Received March 23, 2023;
Accepted manuscript posted July 20, 2023. doi:10.1115/1.4062995

desired front distance. These conditions result in a Reynolds number nearing the transition to turbulence which would be undesirable, and lead the user to select a lower flow rate, 7mL/min, and larger channel width, such as 7 mm.

For conditions where laminar flow is critical, the model helps identify other methods of increasing front distance. For example, inspection of the critical film thickness given by Eq. (5):

$$h_{crit} = \frac{2\,\sigma\cos(\theta)}{\Delta\rho\, g\,[min\,(w, 2L_c)]} \tag{5}$$

suggests that using a lower density solvent or a higher density liquid sub-phase would improve stability of the system. Another possible method would be to use a solvent with a higher surface tension, and to make efforts to minimize the solvent-barrier contact angle.

Another promising method of increasing front distance is to add an additional stabilizing term to the energy balance given in Eq. (9):

$$\frac{v_1^2}{2g} = \frac{v_2^2}{2g} + H_f \tag{9}$$

In this equation, the water surface is assumed to be flat so that the vertical height change may be taken as being insignificant. However, an additional favorable potential energy term could be used to increase front distance. Using the laws of capillary rise between parallel plates [29], a downhill slope can be induced by using a tapered channel that expands in the flow direction. Near the channel entrance the meniscus is pulled up to higher elevation, which introduces a height differential Δh into the energy balance:

$$\frac{v_1^2}{2\,g} + \Delta h = \frac{v_2^2}{2\,g} + H_f \tag{20}$$

This height change can be expressed in terms of the density, ρ_w, contact angle, $\theta_{w,air,}$ and surface tension, $\sigma_{w,air}$ of the supporting fluid (water) with respect to air. The law of capillary rise between parallel plates is applied [29]:

$$\Delta h = \frac{2\,\sigma_{w,air}\cos(\theta_{w,air})}{(\rho_w - \rho_{air})g\,w_1} - \frac{2\sigma_{w,air}\cos(\theta_{w,air})}{(\rho_w - \rho_{air})g\,w_2} = \frac{2\,\sigma_{w,air}\cos(\theta_{w,air})}{(\rho_w - \rho_{air})g}\left(\frac{1}{w_1} - \frac{1}{w_2}\right) \tag{21}$$

Even a small taper added to the channel results in a relatively significant potential energy term. Table 5 shows several combinations of channel widths, where w_1 is the width at the injection point and w_2 is the width near the exit of the channel, and the associated height change Δh. For context, the initial velocity head (i.e., the kinetic energy term) in Eq. (20) for a flow rate of 8 mL/min is only 0.43 mm.

The effect of tapering the channel width was examined experimentally through tests with chloroform. Measurements were made using a channel width near the needle of 1.5 mm that increased to 2.5 mm at the exit, corresponding to a Δh of approximately 3.3 mm. Front distance is measured and overlayed onto the constant channel width results that were shown in Figure 12; these additional results are shown in Figure 14. The dimensionless front distance and pooling parameter for the taper are each calculated using the average channel width of 2 mm for these data. For a given flow rate and average channel gap, the tapered channel

Journal of Fluids Engineering. Received March 23, 2023;
Accepted manuscript posted July 20, 2023. doi:10.1115/1.4062995

provides a significant improvement on front distance, allowing the use of lower flow rates and channel gaps for a given channel length.

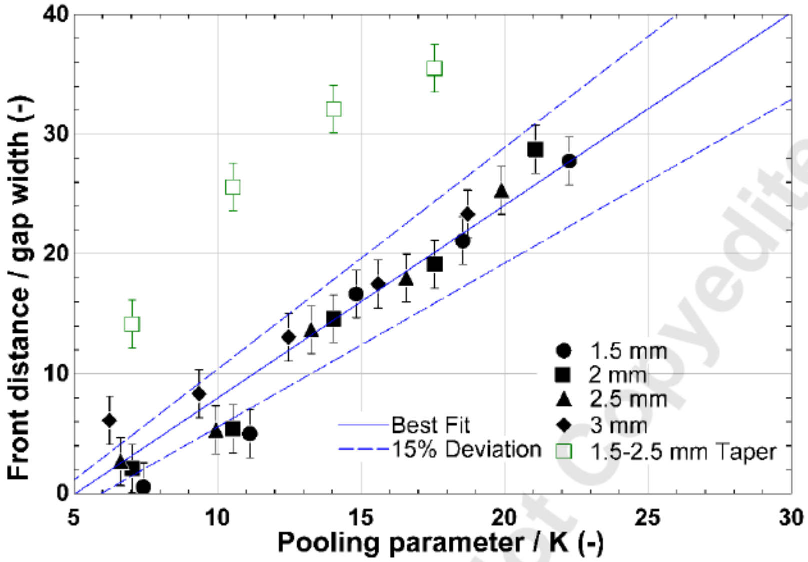

Fig. 14: Front distance normalized by gap width as a function of the pooling parameter over friction factor for chloroform with a straight and tapered channel

The model presented here allows for front distance to be scaled to larger values, which opens the possibility for methods such as TaFISA to be scaled up to larger wafers. An understanding of the physics governing stratified flow within the channel formed between parallel plates helps to define the practical working conditions of solution-based materials processing methods as well as to understand various methods for increasing front distance, such as altering fluid parameters, channel width, and channel geometry.

4 CONCLUSION

Solution-based deposition methods represent a promising route to depositing wafer-scale arrays of aligned CNTs for high speed and low power semi-conductor electronics. Especially promising are solution-based methods that exploit the formation of a 2D nematic liquid crystal at the liquid-liquid interface between water and nanoparticles dispersed in an organic solvent to achieve high packing density and alignment. These methods also present unique challenges that become significant as the process scales, such as the pooling and sinking behavior described here.

The work presented here develops a simple, semi-empirical model that identifies the significant forces governing suspended stratified flow between parallel plates and offers a correlation to predict front distance given a system geometry and fluid parameters. This model is shown to be accurate for multiple fluids to within about ±15% of the experimental data. This correlation can be used to

Journal of Fluids Engineering. Received March 23, 2023;
Accepted manuscript posted July 20, 2023. doi:10.1115/1.4062995

select experimental parameters such as flow rate, channel width, and channel geometry to achieve a desired channel length when scaling solution-based deposition methods. It also suggests an optimal solution space to aid in the design of solution-based materials processing methods where fluids of differing densities are used in contact with one another. Finally, the model was used to identify a method that substantially increases front distance through the introduction of a minor taper to the channel.

The model can be improved to account for changes in channel geometry (e.g., a sudden step change in the channel), changes in channel angle (arranged at 45° with respect to gravity as opposed to vertically) or changes in injection angle. The model could also be improved with further testing using more organic solvents with an apparatus that can test at higher flow rates and channel widths. As solution-based deposition methods for depositing aligned arrays of CNTs and other nanoparticles grow in scale, a deeper understanding of the forces governing the stability of a supported fluid layer will become even more important in the design of reliable, efficient, and practical methods.

ACKNOWLEDGEMENTS

This work was primarily supported by the National Science Foundation (NSF) via SNM-IS Award No. 1727523 (B.P., A.B., M.S.A.). Support is also acknowledged from the Office of Naval Research Award No. N00014-22-1-2843 (S.M.F., M.S.A.). B.P. furthermore acknowledges support from the University of Wisconsin – Madison Fabrication Fellowship Program and the facilities provided by the UW Design and Innovation Labs. Additionally, the authors gratefully acknowledge the use of facilities and instrumentation supported by NSF through the University of Wisconsin Materials Research Science and Engineering Center (DMR-1720415).

REFERENCES

[1] Tulevski, George S., Aaron D. Franklin, David Frank, Jose M. Lobez, Qing Cao, Hongsik Park, Ali Afzali, Shu-Jen Han, James B. Hannon, and Wilfried Haensch. “Toward High-Performance Digital Logic Technology with Carbon Nanotubes.” *ACS Nano* 8, no. 9 (2014): 8730–45. https://doi.org/10.1021/nn503627h.

[2] Franklin, Aaron D., Shu-Jen Han, George S. Tulevski, Mathieu Luisier, Chris M. Breslin, Lynne Gignac, Mark S. Lundstrom, and Wilfried Haensch. “Sub-10 Nm Carbon Nanotube Transistor.” *2011 International Electron Devices Meeting*, 2011. https://doi.org/10.1109/iedm.2011.6131600.

[3] Xu, Lin, Jie Yang, Chenguang Qiu, Shiqi Liu, Weijun Zhou, Qiuhui Li, Bowen Shi, et al. “Can Carbon Nanotube Transistors Be Scaled down to the Sub-5 Nm Gate Length?” *ACS Applied Materials & Interfaces* 13, no. 27 (2021): 31957–67. https://doi.org/10.1021/acsami.1c05229.

[4] Sinha, Sanjeet Kumar, and Saurabh Chaudhury. "Comparative Study of Leakage Power in CNTFET over MOSFET Device." *Journal of Semiconductors* 35, no. 11 (2014): 114002. https://doi.org/10.1088/1674-4926/35/11/114002.

[5] Jinkins, Katherine R., Jason Chan, Robert M. Jacobberger, Arganthaël Berson, and Michael S. Arnold. "Substrate-wide Confined Shear Alignment of Carbon Nanotubes for Thin Film Transistors." *Advanced Electronic Materials* 5, no. 2 (2018): 1800593. https://doi.org/10.1002/aelm.201800593.

[6] Jinkins, Katherine R., Jason Chan, Gerald J. Brady, Kjerstin K. Gronski, Padma Gopalan, Harold T. Evensen, Arganthaël Berson, and Michael S. Arnold. "Nanotube Alignment Mechanism in Floating Evaporative Self-Assembly." *Langmuir* 33, no. 46 (2017): 13407–14. https://doi.org/10.1021/acs.langmuir.7b02827.

[7] Hedberg, James, Lifeng Dong, and Jun Jiao. "Air Flow Technique for Large Scale Dispersion and Alignment of Carbon Nanotubes on Various Substrates." *Applied Physics Letters* 86, no. 14 (2005). https://doi.org/10.1063/1.1897435.

[8] Lay, Marcus D., James P. Novak, and Eric S. Snow. "Simple Route to Large-Scale Ordered Arrays of Liquid-Deposited Carbon Nanotubes." *Nano Letters* 4, no. 4 (2004): 603–6. https://doi.org/10.1021/nl035233d.

[9] Zhao, Mengyu, Yahong Chen, Kexin Wang, Zhaoxuan Zhang, Jason K. Streit, Jeffrey A. Fagan, Jianshi Tang, et al. "DNA-Directed Nanofabrication of High-Performance Carbon Nanotube Field-Effect Transistors." *Science* 368, no. 6493 (2020): 878–81. https://doi.org/10.1126/science.aaz7435.

[10] Liu, Lijun, Jie Han, Lin Xu, Jianshuo Zhou, Chenyi Zhao, Sujuan Ding, Huiwen Shi, et al. "Aligned, High-Density Semiconducting Carbon Nanotube Arrays for High-Performance Electronics." *Science* 368, no. 6493 (2020): 850–56. https://doi.org/10.1126/science.aba5980.

[11] Cao, Qing, Shu-jen Han, George S. Tulevski, Yu Zhu, Darsen D. Lu, and Wilfried Haensch. "Arrays of Single-Walled Carbon Nanotubes with Full Surface Coverage for High-Performance Electronics." *Nature Nanotechnology* 8, no. 3 (2013): 180–86. https://doi.org/10.1038/nnano.2012.257.

[12] Zakri, Cécile, Christophe Blanc, Eric Grelet, Camilo Zamora-Ledezma, Nicolas Puech, Eric Anglaret, and Philippe Poulin. "Liquid Crystals of Carbon Nanotubes and Graphene." *Philosophical Transactions of the Royal Society A: Mathematical, Physical and Engineering Sciences* 371, no. 1988 (2013): 20120499. https://doi.org/10.1098/rsta.2012.0499.

[13] Jinkins, Katherine R., Sean M. Foradori, Vivek Saraswat, Robert M. Jacobberger, Jonathan H. Dwyer, Padma Gopalan, Arganthaël Berson, and Michael S. Arnold. "Aligned 2d Carbon Nanotube Liquid Crystals for Wafer-Scale Electronics." *Science Advances* 7, no. 37 (2021). https://doi.org/10.1126/sciadv.abh0640.

[14] Edomwonyi-Otu, Lawrence C., and Panagiota Angeli. "Pressure Drop and Holdup Predictions in Horizontal Oil–Water Flows for Curved and Wavy Interfaces." *Chemical Engineering Research and Design* 93 (2015): 55–65. https://doi.org/10.1016/j.cherd.2014.06.009.

[15] Keulegan, G.H. "Laminar Flow at the Interface of Two Liquids." *Journal of Research of the National Bureau of Standards* 32, no. 6 (1944): 303. https://doi.org/10.6028/jres.032.016.

[16] Burton, J. C., F. M. Huisman, P. Alison, D. Rogerson, and P. Taborek. "Experimental and Numerical Investigation of the Equilibrium Geometry of Liquid Lenses." *Langmuir* 26, no. 19 (2010): 15316–24. https://doi.org/10.1021/la102268n.

[17] Pujado, P.R, and L.E Scriven. "Sessile Lenticular Configurations: Translationally and Rotationally Symmetric Lenses." *Journal of Colloid and Interface Science* 40, no. 1 (1972): 82–98. https://doi.org/10.1016/0021-9797(72)90175-0.

[18] Phan, Chi M. "Stability of a Floating Water Droplet on an Oil Surface." *Langmuir* 30, no. 3 (2014): 768–73. https://doi.org/10.1021/la403830k.

[19] Vella, Dominic, Duck-Gyu Lee, and Ho-Young Kim. "The Load Supported by Small Floating Objects." *Langmuir* 22, no. 14 (2006): 5979–81. https://doi.org/10.1021/la060606m.

Journal of Fluids Engineering. Received March 23, 2023;
Accepted manuscript posted July 20, 2023. doi:10.1115/1.4062995

[20] Tavana, Hossein, Guocheng Yang, Christopher M. Yip, Dietmar Appelhans, Stefan Zschoche, Karina Grundke, Michael L. Hair, and A. Wilhelm Neumann. “Stick−slip of the Three-Phase Line in Measurements of Dynamic Contact Angles.” *Langmuir* 22, no. 2 (2005): 628–36. https://doi.org/10.1021/la051715o.

[21] Hager, Willi H. “Wilfrid Noel Bond and the Bond Number.” *Journal of Hydraulic Research* 50, no. 1 (2012): 3–9. https://doi.org/10.1080/00221686.2011.649839.

[22] Padding, Johan T., Niels G. Deen, E.A.J.F. (Frank) Peters, and J.A.M. (Hans) Kuipers. “Euler–Lagrange Modeling of the Hydrodynamics of Dense Multiphase Flows.” *Mesoscale Modeling in Chemical Engineering Part I*, 2015, 137–91. https://doi.org/10.1016/bs.ache.2015.10.005.

[23] Rapp, Bastian E. “Chapter 21 - Capillarity.” Essay. In *Microfluidics: Modelling, Mechanics and Mathematics*, 445–51. Elsevier, 2017.

[24] Xiang, Hong Wei. “Chapter 8 - Surface Tension.” Essay. In *The Corresponding-States Principle and Its Practice: Thermodynamics, Transport and Surface Properties of Fluids*, 215–28. Amsterdam: Elsevier, 2005.

[25] White, Frank M., and Henry Xue. “Chapter 6 - Viscous Flow in Ducts .” Essay. In *Fluid Mechanics*, 347–84. New York, NY: McGraw-Hill, 2021.

[26] Traciak, Julian, and Gaweł Żyła. “Effect of Nanoparticles Saturation on the Surface Tension of Nanofluids.” *Journal of Molecular Liquids* 363 (2022): 119937. https://doi.org/10.1016/j.molliq.2022.119937.

[27] Li, Xiaoke, Wenjing Chen, and Changjun Zou. “The Stability, Viscosity and Thermal Conductivity of Carbon Nanotubes Nanofluids with High Particle Concentration: A Surface Modification Approach.” *Powder Technology* 361 (2020): 957–67. https://doi.org/10.1016/j.powtec.2019.10.106.

[28] Nellis, Gregory, and Sanford Klein. “Internal Forced Convection.” Essay. In *Heat Transfer*, 638. Cambridge: Cambridge University Press, 2012.

[29] Bullard, Jeffrey W., and Edward J. Garboczi. “Capillary Rise between Planar Surfaces.” *Physical Review E* 79, no. 1 (2009). https://doi.org/10.1103/physreve.79.011604.

TABLE CAPTIONS

Table 1: Constant parameters

Table 2: Front distance data for chloroform (cm)

Table 3: Averaged front distance (cm)

Table 4: Fluid properties and friction factors of the test fluids

Table 5: Spacer Values and Δh

FIGURE CAPTIONS

Fig. 1: Schematic showing interfacial assembly in TaFISA

Fig. 2: Experimental apparatus. From left to right: (a) the water leveling device, (b) floating stationary post, (c) aluminum plates, (d) linear stage, (e) glass barriers, (f) sacrificial target substrate

Fig. 3: Experimental apparatus showing the needle inserted into the channel. The needle insertion height is measured relative to the water interface. Shown here is a “negative” insertion height (i.e., the needle is above the water); an insertion height of “zero” corresponds to the center of the needle coinciding with the water interface

Fig. 4: Evolution of droplet formation in the TaFISA channel. The scalebar shown is 1 cm

Fig. 5: Schematic of experimental apparatus with the near plate and barrier omitted

Fig. 6: Front distance as a function of needle height for two different flow rates

Fig. 7: Schematic of experimental setup demonstrating the lower and upper limits of channel widths

Fig. 8: Front distance as a function of flow rate for various values of the channel width

Fig. 9: Front distance as a function of channel width for chloroform

Fig. 10: The supported fluid layer slows as friction acts to decelerate the front which causes its height to grow; eventually the critical height is reached which causes pooling to occur

Fig. 11: Dimensionless front distance as a function of pooling parameter for chloroform (black) and chlorobenzene (red)

Fig. 12: Front distance normalized by gap width as a function of the pooling parameter for chloroform and chlorobenzene

Fig. 13: Correlation results from Eq. (17) and data for chloroform front distance as a function of the channel width for various values of flow rate

Fig. 14: Front distance normalized by gap width as a function of the pooling parameter over friction factor for chloroform with a straight and tapered channel

Journal of Fluids Engineering. Received March 23, 2023;
Accepted manuscript posted July 20, 2023. doi:10.1115/1.4062995

TABLES

Table 1: Constant parameters

Parameter	Value
Solvent / Plate Contact Angle	10°
Needle height	0.75 mm
Needle angle relative to horizontal	5°
Needle inner diameter	1 mm

Journal of Fluids Engineering. Received March 23, 2023;
Accepted manuscript posted July 20, 2023. doi:10.1115/1.4062995

Table 2: Front distance data for chloroform (cm)

			Channel Gap (mm)			
			1.5	**2**	**2.5**	**3**
Flow Rate (mL/min)	**2**	**1**	0.0	0.5	0.75	1.5
		2	0.25	0.25	0.5	2.0
		3	0.0	0.5	0.75	2.0
	3	**1**	0.5	1.0	1.25	3.0
		2	1.0	1.0	1.5	1.5
		3	0.75	1.25	1.25	3.0
	4	**1**	2.5	3.0	3.5	3.75
		2	2.25	2.75	3.5	4.0
		3	2.75	3.0	3.25	4.0
	5	**1**	3.0	3.75	4.75	5.5
		2	3.5	4.0	4.25	5.25
		3	3.0	3.75	4.5	5
	6	**1**	4.5	5.75	6.5	7.5
		2	3.75	5.5	6.5	6.5
		3	4.25	6.0	6.0	7.0
	7	**1**	5.0	7.25	n/a	n/a
		2	4.75	6.75	n/a	n/a
		3	4.75	7.5	n/a	n/a
	8	**1**	7.0	n/a	n/a	n/a
		2	7.5	n/a	n/a	n/a
		3	6.75	n/a	n/a	n/a

Journal of Fluids Engineering. Received March 23, 2023;
Accepted manuscript posted July 20, 2023. doi:10.1115/1.4062995

Table 3: Averaged front distance (cm)

		Channel gap (mm)			
		1.5	**2**	**2.5**	**3**
Flow Rate (mL/min)	**2**	0.08	0.42	0.67	1.83
	3	0.75	1.08	1.33	2.50
	4	2.50	2.92	3.42	3.92
	5	3.17	3.83	4.50	5.25
	6	4.17	5.75	6.33	7.00
	7	4.83	7.17	n/a	n/a
	8	7.08	n/a	n/a	n/a

Journal of Fluids Engineering. Received March 23, 2023;
Accepted manuscript posted July 20, 2023. doi:10.1115/1.4062995

Table 4: Fluid properties and friction factors of the test fluids

	Chloroform	Chlorobenzene	Water
Density (ρ)	1.5 kg-m^{-3}	1.1 kg-m^{-3}	1.0 kg-m^{-3}
Dynamic viscosity (μ)	0.55 mPa-s	0.80 mPa-s	1.0 mPa-s
Static Contact Angle (θ)	10°	10°	10°

Journal of Fluids Engineering. Received March 23, 2023;
Accepted manuscript posted July 20, 2023. doi:10.1115/1.4062995

Table 5: Spacer Values and Δh

w_1(mm)	w_2(mm)	Δh(mm)
1.5	1.5	0
1.5	2	2.0
1.5	2.5	3.3
1.5	3	4.1
1.5	3.5	4.6